

A machine learning based approach for better prediction of fatigue life of offshore wind turbine foundations using smaller datasets

Ahmed Mujtaba¹, Wout Weijtjens¹, Negin Sadeghi^{1,2}, and Christof Devriendt^{1,2}

¹OWI-Lab, AVRГ, Vrije Universiteit Brussel (VUB), Brussels, 1050, Belgium

²24SEA, Brussels, 1000, Belgium

Correspondence: Ahmed Mujtaba (ahmed.mujtaba@vub.be)

Abstract.

As offshore wind turbine (OWT) foundations approach the end of their design life, the industry is increasingly focused on strategies for lifetime extension. As fatigue is the design driver for foundations of OWTs, reliable fatigue damage predictions are essential to support informed decisions for lifetime extensions. While simulation-based fatigue life reassessments are common, data-driven approaches using measured strain data have emerged as an alternative that can reduce modeling uncertainties. But, data-driven approaches face challenge as having access to strain data over the entire past lifetime is not an industry-standard. Often measurement campaigns are only kicked off when a lifetime extension is considered, thus limiting the availability of strain data. However, environmental and operational conditions (EOCs) of the wind turbines are usually recorded during the whole operational period. Using limited strain measurements and long term EOCs to estimate fatigue damage in unmonitored periods during the lifetime of the turbine requires temporal extrapolation techniques. Existing work on this topic presents several extrapolation methods, including linear time-based extrapolation, binning based on correlations between EOCs and average damage, and machine learning (ML) models. The accuracy of these methods depends on factors such as the selected EOC parameters, the duration and starting point of available strain data, the power rating and type of the wind turbine, as well as the type and architecture of the extrapolation model used. This study presents a novel machine learning based extrapolation model using random forest (RF) for temporal extrapolation of strain measurements. A comparative analysis of novel RF model with previously identified binning models is presented. The extrapolation performance is validated using five years of measured strain, SCADA, and wave data from a 3 MW and a 9 MW OWT installed on monopile foundations in the Belgian North Sea. Using a sliding window approach on the available monitoring data, we estimate and compare the statistical uncertainty in fatigue life predictions of various extrapolation models. The results indicate that wave parameters play a more significant role in fatigue prediction for larger turbine of 9 MW compared to smaller one of 3 MW power rating. For limited data sizes, less than 12 months, the proposed RF model demonstrates superior performance, offering more reliable fatigue life predictions with reduced statistical uncertainty. However, for longer datasets, greater than 12 months, the performance advantage of RF model over binning methods becomes less pronounced. [For 3 MW OWT with datasets greater than 18 months, RF model is outperformed by binning methods.](#)

1 Introduction

As offshore wind farms mature, extending the operational lifetime of wind turbines has become a pressing concern for the wind energy industry. According to WindEurope (2017), a substantial share of the installed wind capacity in the European Union is expected to reach the end of its design life between 2020 and 2030. Decommissioning these assets without extending their service would hinder progress toward the EU’s 2030 target of achieving 50% of electricity from renewable sources. Therefore, lifetime extension, alongside repowering and new installations, is vital for meeting long-term sustainability goals. As highlighted by Shafiee (2024), extending the operational life of OWTs offers significant economic and environmental benefits, including reduced Levelized Cost of Energy (LCOE) and lower emissions.

Fatigue is a governing factor in the structural design of wind turbine support structures, which are primarily optimized for dynamic—rather than static—loading conditions (Sparrevik (2019)). Monopile foundations are typically designed for a service life of 20–25 years. However, findings from some structural health monitoring (SHM) campaigns suggest that actual fatigue loads may be lower than anticipated, revealing unexploited fatigue capacity and motivating detailed reassessments for lifetime extension purposes (Tewolde et al. (2018)). For example, in the case of lifetime extension of the Samsø offshore wind farm in Denmark, the Danish Energy Agency required detailed fatigue reassessments using updated load conditions to support lifetime extension permits (Buljan (2025)). International guidelines for lifetime extension, such as those outlined in DNV-ST-0262 (2016), recommend fatigue life reassessments based on updated models that incorporate measured environmental and operational data. While traditional fatigue reassessments rely heavily on simulation-based models, the availability of measured strain, as typically provided by SHM systems, and long term EOC data opens the door for data-driven alternatives that can reduce uncertainties associated with initial design assumptions in the simulation based models (Kinne and Thöns (2023)).

To support lifetime assessments, two primary approaches exist: simulation-based reassessments using updated models, and data-driven methods using measured strains. The latter mitigates modeling assumptions but introduces new challenges— such as high cost of installation and maintenance of strain gauges on OWTs (Bezziccheri et al. (2017)) and limited data availability (Pacheco et al. (2023)). Strain gauges are typically installed at a few critical locations, requiring spatial extrapolation to predict strains at locations where no direct measurements are available. Strain measurements are limited in duration as having strain data over the entire past lifetime is not an industry-standard and because of the challenges associated with traditional sensor deployment in harsh marine environments, such as sensor failures due to corrosion caused by saltwater and humidity, and high costs related to complex installation logistics (Ángel Encalada-Dávila et al. (2025)). Often measurement campaigns are only started when a lifetime extension is considered, thus limiting the availability of strain data. On the other hand, a Supervisory Control and Data Acquisition (SCADA) system is typically installed on OWTs to capture and record EOCs such as wind speed, power, rotational speed etc., to enable the wind farm operators to track and control the turbines performance in real time (Moynihan et al. (2024)). The available data paves the way for temporal extrapolation techniques that use limited strain measurements and long term EOCs to estimate fatigue damage in unmonitored periods during the lifetime of the turbine.

Prior research has extensively explored extrapolation of strain and load data for offshore wind turbines, both spatially, to uninstrumented locations, and temporally, beyond the measurement window. Spatial extrapolation studies include those targeting different positions on the same turbine (Ziegler et al. (2019); Moynihan et al. (2024); Fallais et al. (2025); Ziegler et al. (2017); Zou et al. (2023); Zhang et al. (2024); Simpson et al. (2025); Ángel Encalada-Dávila et al. (2025)), as well as farm-wide extrapolation approaches where measurements from one or a few instrumented turbines, called fleet leaders, are extended to others across the farm (de N Santos et al. (2024); Weijtens et al. (2016); Noppe et al. (2020); Pacheco et al. (2023)).

Temporal extrapolation methods vary in complexity, ranging from simple linear techniques to binning strategies that relate fatigue damage to EOCs, and more advanced ML approaches. Notable studies have assessed the accuracy of these methods using various datasets (Hübler and Rolfes (2022); Ziegler and Muskulus (2016); Weijtens et al. (2016)). For example, Hübler et al. (2018) evaluates linear extrapolation, also called 0-dimensional (0d) binning, 1d binning, where 10-minute fatigue damage is split into wind speed bins, and 2d binning, splitting fatigue damage into wind speed and wind direction bins using strain measurements from a 3MW OWT installed on a monopile. Hübler et al. (2018) concludes that strain measurements of 9 to 10 months provide a representative and unbiased dataset with 1d binning using wind speeds giving the most reliable fatigue life estimations. Hübler and Rolfes (2022) studies the performance of multi-dimensional binning extrapolation, Artificial Neural Networks (ANN) and Gaussian Process Regression (GPR) trained using multiple 1-year periods of measured strains. In Hübler and Rolfes (2022), binning approaches using wind speed correlations provide best results. Pacheco et al. (2022) summarizes the steps for calculating and extrapolating fatigue damage in wind turbines using strain measurements. Apart from estimating fatigue life of instrumented turbine, Pacheco et al. (2022) concludes that the results from instrumented turbines can be extrapolated to uninstrumented turbines in the same wind farm. Pacheco et al. (2023) uses a damage capture matrix formed using 2d binning in wind speed and turbulence intensity, to extrapolate strain measurements from one turbine to other turbines in an onshore wind farm. Pacheco et al. (2023) recommends using 1-year monitoring period and concludes that the uncertainties in extrapolations decrease with increasing monitoring period.

The rapid development and advances in computer science and its applications in wind energy pose machine learning models as a favorable option for temporal extrapolation of fatigue damage in wind turbines (He et al. (2022); Raju et al. (2025)). Literature focuses on using ML models as surrogates trained on simulated data to predict fatigue loads on each turbine in a wind farm (Bossanyi (2022); Gasparis et al. (2020); Singh et al. (2022)). There is limited literature on use of ML models trained on strain measurements and used for fatigue damage predictions such as de N Santos et al. (2023) uses Physics-guided learning of neural networks trained on 9 months of strain measurements for long-term fatigue damage estimation using SCADA and acceleration data. In wind energy applications, Random Forest model is proved to be a powerful ensemble learning method, widely used for regression and classification tasks. RF models adapt excellently to high-dimensional data and large-scale datasets, and are robust in dealing with missing values and unbalanced datasets (Karadeniz (2025)). For example, Karadeniz (2025) compares RF, Long Short-Term Memory Network (LSTM) and Gated Recurrent Unit (GRU) for predicting Total Harmonic Distortion Voltage (THDV) of offshore wind farms to conclude that RF models outperforms LSTM and GRU in predicting THDV with lowest root mean squared error (RMSE). Similarly, Zhou et al. (2016) uses RF regression model to

predict short term power production of a wind farm and Rouholahnejad and Gottschall (2025a) uses RF model to extrapolate near surface wind speed up to 200m.

Literature review highlights that the sensitivity of ML and binning based extrapolation models to different turbine power ratings remains poorly understood. Many studies assume homogeneity in turbine design and operating conditions, often focusing on a single turbine type and neglecting spatial variability across the farm (Bouty et al. (2017)). Consequently, it is unclear how extrapolation performance varies across turbines with different power ratings, or environmental exposures.

Moreover, validation of these models is often limited to short timescales (e.g., several months), which restricts confidence in their long-term predictive capability. While several binning-based and regression-based methods have been proposed (Ziegler et al. (2017); Pacheco et al. (2023); Sadeghi et al. (2023b)), their comparative effectiveness and robustness under varying data availability, input features, and turbine power ratings are not yet well established. Especially in discussions of lifetime extension for aging turbines, methodologies that require shorter measurement campaigns are advantageous. This raises key questions like: What is the minimum duration of the monitoring period required for statistically reliable fatigue life predictions? and Can machine learning models reduce this monitoring period without sacrificing accuracy or increasing uncertainty?

Despite the increasing attention to data-driven extrapolation, key gaps remain in the literature:

- A systematic comparison of binning and machine learning, specifically random forest, models for fatigue life prediction across multiple turbine sizes is missing.
- The relative importance of SCADA and wave parameters selection for these models to predict fatigue damage has not been thoroughly assessed for turbines of different power ratings.
- The ability of these models to predict fatigue damage across different directions (fore-aft, side-side, or single-sensor measurements) has not been thoroughly evaluated for turbines of varying capacities.
- The sensitivity of these models to data availability, including variations in dataset size and measurement start time, is underexplored.

While previous studies have compared binning approaches with machine learning models such as ANNs and GPR (Hübler and Rolfes (2022)), these comparisons were generally performed for a single turbine and often using relatively limited datasets. Similarly, earlier work has examined the sensitivity of data-driven fatigue extrapolation to dataset length and measurement start time (Hübler and Rolfes (2022)), but again typically for a single turbine. Consequently, a systematic evaluation of Random Forest models across multiple turbine sizes using extensive monitoring data, together with a multi-directional assessment of model performance and parameter relevance remains missing.

This study addresses these gaps by first introducing a novel ML based extrapolation model using random forest for temporal extrapolation of strain measurements. This model is compared with state-of-the-art temporal extrapolation techniques for fatigue life prediction and validated using five years of measured strain, SCADA, and wave data from two offshore wind turbines: a 3 MW and a 9 MW turbine, both installed on monopiles in the Belgian North Sea. We analyze the influence of dataset size, measurement start time, model dimensionality, and feature selection on extrapolation accuracy. Multiple configurations

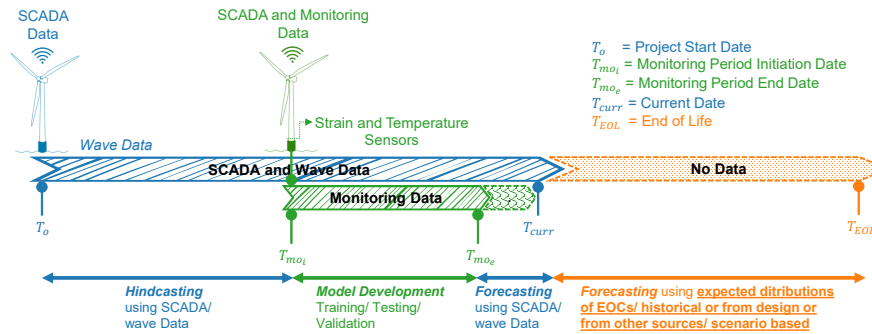


Figure 1. A timeline showing model developed using monitoring data used for hind-casting and forecasting using SCADA-wave data where available, and forecasting in future using expected distributions of EOCs

125 of random forest models are tested, including recursive feature elimination with cross-validation (RFECV) and state-specific modeling, to explore trade-offs between model complexity and predictive performance.

The findings provide new insights into the reliability, convergence behavior, and practical limitations of data-driven fatigue extrapolation models, offering valuable guidance for their deployment in support of lifetime extension assessments.

130 The remainder of the paper is structured as follows: It begins with the Objective section, leading into the Measurement Setup for strain, collecting SCADA, and wave data. The paper then explains the Methodology section. This section elaborates on model development with a focus on feature selection, binning, and the RF model, outlines the technique for statistical uncertainty estimation applicable to these extrapolation models and details the approach for damage extrapolation used in estimating fatigue life. The paper then concludes with a presentation of Results of fatigue lifetime predictions in various directions along with discussions of the results.

135 2 Objective

Consider initiating a strain measurement campaign aimed at reassessing the fatigue life of OWT with the goal of extending their lifetime. How long should measurements be conducted to ensure a reliable estimate of fatigue life? The growing number of aging OWTs demands fast, reliable, and data-efficient methods to accurately predict their end-of-life (EOL). Addressing this question is important since it can result in reduced costs for prolonged measurement campaigns and more time-efficient fatigue life estimates. Precise predictions of fatigue life are essential for making informed lifetime extension decisions; however, this requires balancing the duration of measurement campaigns with both the financial costs of data acquisition and the accuracy of the predictions.

Figure 1 illustrates the typical scenario encountered in fatigue life estimation. A strain sensor is installed at a later stage of turbine's operation, for example when lifetime extension is considered, initiating a monitoring period between T_{moe} and T_{moe} .
 145 The shaded green region between T_{moe} and T_{curr} indicates that the monitoring campaign may end before the current date.

This represents the period for which no strain measurements are available. In cases where monitoring is still ongoing T_{mo_e} and T_{curr} coincide. Meanwhile, SCADA and wave data are usually available from the turbine's commissioning at T_o . During the monitoring period $\Delta T_m = T_{mo_e} - T_{mo_i}$, extrapolation models are trained/tested and validated using measured strain and corresponding SCADA/wave data. These models are then used to estimate cumulative fatigue damage up to the projected end-of-life time T_{EOL} , leveraging either historical SCADA/wave records or design-based EOC distributions. Such models can also facilitate scenario-based forecasting of fatigue damage under varying operational profiles.

This study presents a ML based extrapolation technique using RF models and systematically investigates the uncertainty in fatigue life predictions under varying monitoring periods and starting points. Given the seasonality of EOCs, the timing and length of the data window can significantly influence model robustness. In addition, factors such as binning strategies (e.g., dimensionality, bin resolution, empty-bin handling) and feature selection techniques in ML-based models play a critical role in the extrapolation accuracy.

Using long-term strain, SCADA, and wave measurements from two OWTs installed on monopiles—this study aims to:

- Quantify the minimum monitoring duration ΔT_m required for reliable fatigue life predictions using ML and binning extrapolation models.
- Develop robust estimates of turbine end-of-life T_{EOL} using extrapolation models based on measured strain and EOCs data.
- Estimate uncertainty bounds associated with T_{EOL} under different modeling approaches.
- Evaluate the potential of machine learning models, Random Forests, to reduce required monitoring durations and improve prediction reliability, in comparison to traditional extrapolation methods such as linear and binning-based models.
- Compare the performance of different extrapolation models across varying offshore wind turbine power ratings, 3 MW and 9 MW, to assess model reliability.
- Compare the ability of these models to predict fatigue damage across different directions, fore-aft, side-side, or single-sensor measurements, and for turbines of different power ratings, 3 MW and 9 MW.

3 Measurement Setup

Table 1 provides an overview of the parameters used in this study along with the data availability. 5 years of strain measurements, SCADA and wave data from a 3MW and 9MW OWT are used. The strain measurement setup consists of six circumferential strain gauges installed on the transition piece (TP) near the tower-TP interface. Figure 2 presents the windrose diagrams for the 3 MW and 9 MW OWT, illustrating the probability distribution of wind occurrence across different directions. Figure 2 also shows the sensor locations along the circumference and positioned around the circumference, together with the dominant wind direction of 230° for both turbines. The closest sensor. The difference in windrose size reflects the actual

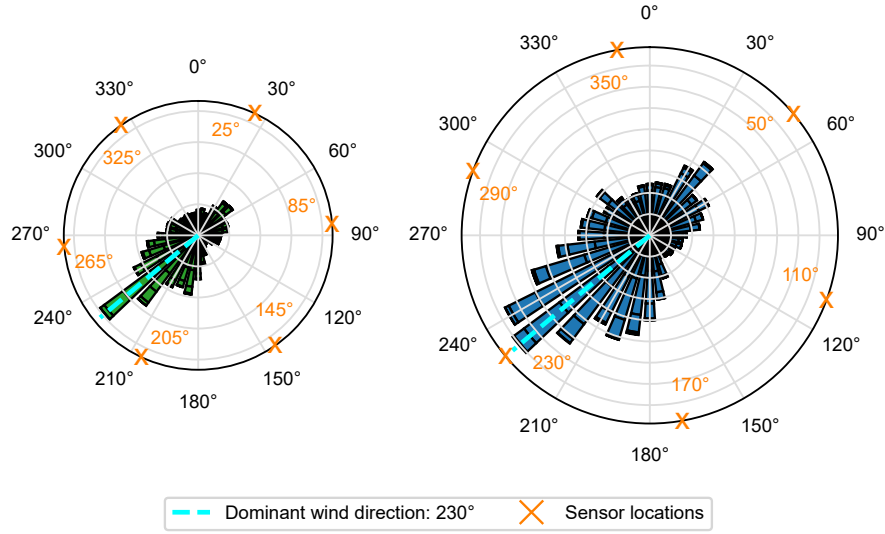


Figure 2. Sensors location and windrose showing dominant wind direction for a 3MW (left) and 9MW (right) OWT

relative monopile diameters: the smaller windrose on figure 2 (left) corresponds to a smaller diameter monopile for the 3 MW OWT, while the larger windrose on figure 2 (right) represents the larger diameter monopile of the 9 MW OWT. The sensor closest to the dominant wind direction is located at 205° for 3MW OWT and the 3 MW OWT and at 230° for 9MW the 9 MW OWT.

180 3.1 Strain data

The data from six circumferential ~~strain sensors~~ electrical strain gauges is pre-processed using the steps shown in Fig. 3. ~~The strain measurements are converted to stress using Hooke's Law. The stress measurements per sensor are then used to calculate stresses.~~ Each strain gauge is installed together with a dedicated thermocouple to enable temperature compensation. This temperature compensation as well as any long-term measurement drift is addressed through continuous follow-up and periodic recalibration of the strain gauges data by the SHM hardware supplier.

From the measured strains at the six circumferential sensors, the corresponding stresses and bending moments are obtained through a two-step procedure. First, the axial stress at each sensor location is computed using Hooke's law (Equation (1)).

$$\sigma_{zz,j} = E \varepsilon_{zz,j}, \quad (1)$$

where E is Young's modulus, and $\varepsilon_{zz,j}$ and $\sigma_{zz,j}$ are the measured axial strain and resulting axial stress at the j -th sensor, respectively. The general equation for normal stress $\sigma_{zz,j}$ induced by a normal force F_N and global bending moments M_{NS} (North-South) and M_{EW} (East-West) in cylindrical coordinates is given by Equation 2.

$$\sigma_{zz,j} = \frac{F_N}{A} + R_i \left[\frac{M_{NS}}{I_C} \sin(\theta_j) - \frac{M_{EW}}{I_C} \cos(\theta_j) \right], \quad (2)$$

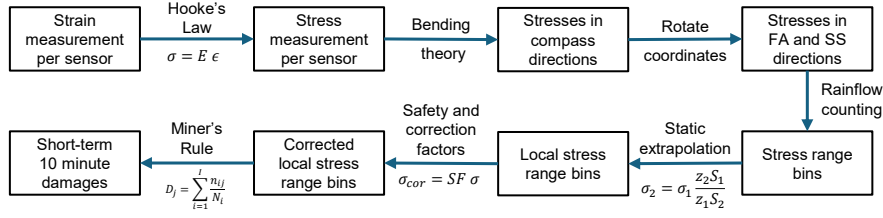


Figure 3. Strain data preprocessing to calculate short-term ~~10-minute~~ 10-minute damages in FA and SS directions (Image reproduced from Hübler et al. (2018))

195 where A is the cross-sectional area, R_j is the inner radius at the sensor location, I_C is the area moment of inertia, and θ_j is the clockwise angular position of the j -th sensor from north-south axis. Equation 2 can be written for each sensor. With six sensors, this formulation yields an overdetermined system that is solved using a least-squares fitting procedure to estimate the normal load F_N and bending moments in both directions M_{NS} (North-South) and M_{EW} (East-West) from the measurements (see Sadeghi et al. (2023a) and Link and Weiland (2014) for more details).

The resulting bending moments are then rotated in fore-aft (FA) and side-side (SS) ~~directions which are de-facto standard loading directions in wind turbines.~~ Each 10 minute direction using Equation 3.

$$200 \begin{Bmatrix} M_{FA} \\ M_{SS} \end{Bmatrix} = \begin{bmatrix} \cos(-\psi + \pi) & \sin(-\psi + \pi) \\ -\sin(-\psi + \pi) & \cos(-\psi + \pi) \end{bmatrix} \begin{Bmatrix} M_{NS} \\ M_{EW} \end{Bmatrix}, \quad (3)$$

where ψ is the mean yaw angle within each 10-minute interval. This transformation yields the fore-aft (M_{FA}) and side-side (M_{SS}) bending moments, also defined as normal bending moment (M_{in}) and lateral bending moment (M_{ll}) respectively in IEC61400-13 (2021).

205 Stresses in fore-aft direction refer to axial stresses caused by fore-aft bending moment (M_{FA}) and stresses in side-side direction refer to axial stresses caused by side-side bending moment (M_{SS}). Each 10-minute signal is processed using rainflow cycle counting to get stress range histogram.

Stress range histograms or cycle count matrices are scaled using a combination of static extrapolation, safety, and correction factors. The static extrapolation factor is employed to project the measured stress signals onto fatigue-critical structural locations, without modeling structural dynamics. This factor is computed as the product of two ratios: (i) the bending moment ratio between the extrapolated and measured locations, obtained from bending moment diagrams either in design documentation or reanalysis; and (ii) the section modulus ratio at the two locations.

215 Additional correction factors include a stress concentration factor (SCF) as defined in DNV-RP-C203 (2024) for various fatigue details, a material safety factor (MSF) usually defined in as specified in relevant design guidelines such as IEC-61400-1 (2019), and a thickness correction factor following DNV-RP-C203 (2024) guidelines the recommendations in DNV-RP-C203 (2024) to account for the size effects. These factors are applied to generate a corrected stress range histogram for fatigue damage anal-

ysis. However, the exact numerical values of these scaling factors are not essential for the temporal extrapolation process and do not affect the conclusions of this paper (-Hübler and Rolfes (2022)).

Subsequently, the fatigue damage corresponding to each stress range bin is computed using the appropriate S-N (Wöhler) curve described by Basquin Equation 4 (BASQUIN (1910)), where $\log(\bar{a})$ is the intercept term and m is the slope (or Wöhler
220 exponent) of the SN curve, $\Delta\sigma$ is the stress range and N is the number of cycles to failure.

$$\log(N) = \log(\bar{a}) - m \cdot \log(\Delta\sigma) \quad (4)$$

The slope (m) and intercept ($\log(\bar{a})$) defining the S-N curve depend on the fatigue detail, environmental conditions, and material properties, and are provided in DNV-RP-C203 (2024) guidelines. In this study, the bilinear DNV D-A curve for a D-detail (circumferential butt weld made from both sides) is adopted, with slopes of $m = [3, 5]$ and intercepts of $\log(\bar{a}) = [12.164, 15.606]$,
225 with a transition at 10^7 cycles.

The individual damage contributions are calculated and accumulated over time using Palmgren-Miner's linear damage rule (Miner (1945)) to estimate the fatigue damage per 10-minute interval, as shown in Equation 5.

$$D = \sum_{i=1}^k \frac{n_i}{N_i} \quad (5)$$

where:

- 230 – n_i is the number of cycles in the i^{th} stress range bin,
- N_i is the number of cycles to failure at the i^{th} stress range (obtained from the S–N curve),
- k is the total number of stress range bins.

10-minute fatigue damage is used as the extrapolation models target variable. Strain data processing, cycle counting, stress range corrections, fatigue damage calculation and accumulation are done using open source python package py-fatigue
235 (D'Antuono et al. (2023)). In this study, fatigue life is estimated using three approaches based on damage values:

- **Single Sensor Damage:** Fatigue life is estimated using damage calculated from the sensor nearest to the dominant wind direction. This approach bypasses the rotation of stress measurements and directional compass transformation (see Fig. 3), applying rainflow counting directly to the raw stress time series.
- 240 – **Fore-Aft (FA) Damage:** It is assumed that the turbine faces fore-aft damage conditions throughout its lifetime. This method ~~is conservative and~~ likely underestimates fatigue life as compared to single sensor, since FA damage state is not constantly maintained over time.
- **Side-Side (SS) Damage:** It is assumed that only side-side damage prevail throughout turbine lifetime. This approach allows estimation of life consumption if SS damage states were persistent.

The methodology used to extrapolate damage predictions and estimate fatigue life (T_{EOL}) is described in detail in [Sectionsection 4.3](#).

Table 1. Overview of SCADA, wave and strain parameters for 3MW and 9MW OWT, their sources, duration and availability factors

	Sensor	Statistic	Variable	Symbol	Units	Data Availability (%) [3MW]*	Data Availability (%) [9MW]**
Inputs	SCADA	10-minutes mean	Wind speed	WS	m/s	99.87	98.22
			Yaw Angle	WD	°	99.87	98.48
			Pitch Angle	PI	°	99.87	97.81
			Power	PW	kW	99.74	98.3
			Rotational Speed	RPM	rpm	99.87	98.62
			Turbulence Intensity	TI	-	98.66	98.22
			Operational State†	OS	-		
Wave Data		30-minutes mean	Mean Wave Height	WH	cm	99.98	99.98
			Mean Wave Period	WP	s	99.98	99.98
			High Frequent Wave Direction	HF	°	99.96	99.97
			Low Frequent Wave Direction	LF	°	99.96	99.97
			Tidal level***	TL	cm	100	100
Fatigue Target	Strain Gauges	10-minutes fatigue damage	Single Sensor Damage		-	96.92	97.78
			Fore-Aft Damage	FA	-	96.77	96.02
			Side-Side Damage	SS	-	96.77	96.02

* 5 years of monitoring and SCADA data used 2020-01-01 till 2024-12-31

** 4.67 year of monitoring and SCADA data used 2020-05-01 till 2024-12-31

*** Tidal levels are taken from Ostend harbour - Tide due to lower data availability for Wandelaar Measuring pile [all other wave data taken from Thorntonbank South Buoy]

†Operational States for 3MW 'nominal', 'transient', 'idling', 'highwind'

Operational States for 9MW 'nominal', 'transient', 'idling', 'highwind', 'curtailed'

245 3.2 SCADA and wave data

The SCADA system provides essential turbine parameters including wind speed, yaw angle, pitch angle, rotor power output, and rotational speed. The corresponding symbols used for these variables throughout this study are summarized in Table 1. 10-minute mean statistics of these parameters are utilized as inputs for extrapolation models development.

Turbine operational states defined based on the SCADA-10-minute SCADA statistics including nominal, idling, highwind, ~~abnormal curtailed~~ (only for ~~9MW OWT~~), ~~curtailed and invalid~~ 9 MW OWT) and transient are incorporated into both binning and ML based extrapolation models. ~~Invalid operational states refer to intervals lacking valid SCADA-derived statistics, typically involving transient events such as rotor start-up or shut-down.~~ Intervals that occur during turbine transients (e.g. start-up or shut-down, shutdown) fall outside the predefined statistical thresholds on SCADA statistics and are therefore labeled transient. For the 9 MW OWT, an additional ~~abnormal curtailed~~ operational state is identified, associated with curtailed power output, defined as intentional operation of the turbine at reduced power output to satisfy grid requirements. The *nominal* power generation and *idling* (Parked) operational states are defined consistently across both the 3 MW and 9 MW OWTs.

Turbulence intensity (TI) is computed for each 10-minute interval using the ratio of the standard deviation to the mean wind speed, defined as:

$$TI = 100 \times \left(\frac{\sigma_{\text{wind speed}}}{\mu_{\text{wind speed}}} \right) \quad (6)$$

Wave and tidal data are typically not included in wind farm SCADA datasets. For this study, publicly available environmental data from the Meetnet Vlaamse Banken (MVB (2025)) covering the Belgian part of the North Sea are used. Meetnet Vlaamse Banken comprises wave buoys and measurement piles deployed across the North Sea, providing measurements of wind, wave, and tidal conditions. Reported wave characteristics include wave height, 10% highest waves, height of waves with period greater than 10 seconds, high frequent wave direction, low frequent wave direction, average wave period and tidal levels. These measurements are generally reported with sampling frequency of 15–30 minutes and are resampled with interpolation to align with the 10-minute resolution of SCADA measurements from OWTs.

Wave data from the Thorntonbank South buoy are selected for analysis, as this station offers high data availability during the study period and is geographically closest to the considered wind farms having a distance of 18.5 km from 3 MW OWT and 7.8 km from 9 MW OWT. Although this location does not provide tidal data, tidal measurements from the Wandelaar station were evaluated but excluded due to a low data availability during the time of interest. Instead, tidal data from the Oostende station are used, as they align well with wave radar observations at one of the wind farms analyzed of which a small window was available for validation. A potential time offset exists between wave events at the OWT site and the measurement station due to spatial separation. A simplified time-shift estimation, assuming deep-water wave propagation and direct travel from the buoy to the turbine location, yields a maximum offset of approximately 40 minutes. However, no explicit correction for wave time offset is applied in this study. The distance between the turbine and the wave measurement buoy leads to some differences in wave parameters compared with measurements taken closer to the 9 MW turbine, although the overall temporal trends remain consistent. However, the acceptable distance between wave measurement station and a turbine depends on local bathymetry and wave climate, and closer measurements may be required in areas with strong spatial gradients.

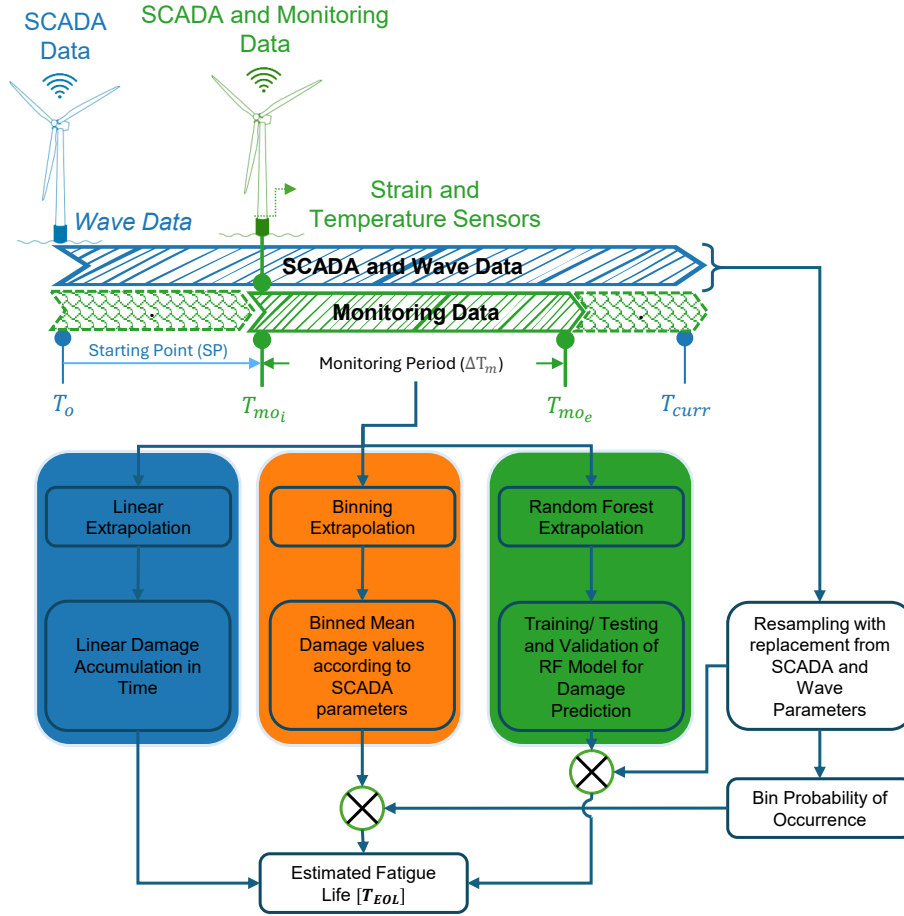


Figure 4. 5 years of data $T_{curr} - T_0$ is split into a sliding window of variable size ΔT_m and starting point SP used for models development. Fatigue life T_{EOL} is estimated using complete SCADA and Wave data.

4 Methodology

280 Figure 4 illustrates an overview of the methodology, where various extrapolation models are applied to different monitoring period sizes and starting points. A selected monitoring window ΔT_m , with varying durations and starting points, is used to train extrapolation models. These models predict 10-minute fatigue damage based on SCADA/ wave parameters which is used to estimate fatigue life T_{EOL} over the full operational timeline.

4.1 Model Development

285 Two modeling approaches are investigated for fatigue life extrapolation: (1) multi-dimensional binning (Pacheco et al. (2022); Hübler et al. (2018); Hübler and Rolfes (2022); Sadeghi et al. (2023b)), and (2) Random Forest Model. The Random Forest

model has been selected owing to its robustness and better performance relative to other machine learning models (Karadeniz (2025); Rouholahnejad and Gottschall (2025a)). This paper focuses on the fundamental question as to whether the deployment of ML models offers any significant benefits instead of comparing the performance of various ML models.

290 ~~10-minute~~-10-minute SCADA and wave statistics are used as input parameters and 10-minute fatigue damage is the target variable as summarized in Table 1. Extrapolation models are evaluated under varying monitoring durations and feature subsets to assess their robustness and prediction accuracy.

4.1.1 Feature Selection

Feature selection is a crucial step, especially in fatigue modeling where input parameters, to be precise the SCADA and wave data, may vary in importance depending on the operational state of the turbine and the size of the training dataset. Feature selection is performed for both the binning and RF models to enable a fair comparison by using the same set of input features. Four approaches to feature selection are employed:

1. **Random Forest Feature Importance:** A filter-based method is applied using the built-in feature importance metric from a Random Forest model~~trained on~~, which ranks input variables based on their contribution to reducing node impurity across all trees (see Breiman (2001, 2002) for more details). This model is trained using the first 12 months of monitoring data. The top five features, capturing over 80% of cumulative importance, are selected. This 5-feature limit enables a fair comparison between a 5-dimensional binning approach and RF model using five features, denoted by RF-5D. Feature selection is performed separately for different fatigue targets, fore-aft, side-side, and single sensor damage, since the relevance of features differs for these damage types. Categorical variables, such as turbine operational states, are transformed using one-hot encoding to enable their use in tree-based models.
2. **Global RFECV:** A recursive feature elimination with cross-validation (see Guyon et al. (2002) for details on RFECV methodology) is applied globally, i.e., across all operational states, using the same 12-month dataset. This method, referred to as Global RFECV, aims to identify a reduced yet effective feature subset optimized for overall model performance.
3. **State-Specific RFECV:** To account for operational state-dependent fatigue behavior, RFECV is applied individually to each turbine operational state, generating unique feature subsets per state. Separate Random Forest models are trained for each state, significantly increasing the number of models but allowing for tailored fatigue prediction.
4. **Full-Feature Baseline:** A baseline model using all available features is also developed to serve as an upper-bound benchmark, against which performance of RF-5D and RFECV-based models is compared.

315 4.1.2 Binning Extrapolation

In the binning approach, fatigue damage values are discretized based on selected EOC parameters. A single statistic, typically mean, is computed to represent all damage in each bin, resulting in a multi-dimensional damage matrix. To estimate long-term

fatigue life, EOC parameters are sampled from extended operational periods to determine bin probabilities. These probabilities, representing the occurrence likelihood of EOCs, are combined with the damage matrix to compute the expected fatigue damage.

320 To account for varying turbine operational states, the monitoring period ΔT_m is first segmented by operational states, and a separate damage matrix is constructed for each state. This allows the binning approach to accurately reflect state-dependent fatigue behavior.

In this paper, the dimensionality of binning is increased from 1D to 5D. In 1D binning, only wind speed is used if wind speed is in the selected features. This is because Hübler and Rolfes (2022) suggests that binning approaches using wind speed correlations provide best results. For 2D binning, wind speed along with the parameter with the highest importance, as

325 determined by feature_importances_ scores from a random forest model, is used for discretization. For higher dimensions, the top-ranked features are sequentially added—e.g., 3D binning uses wind speed and the top two features, 4D binning uses wind speed and the top three features, and so on, up to 5D.

Explicit bin size optimization is not performed in this study. [Bin sizes for SCADA and wave parameters used in this paper are given in Appendix D.](#) A critical challenge in multi-dimensional binning is the treatment of empty bins, which can arise due to data sparsity in high-dimensional feature spaces. For example in 3D binning based on wind speed, wind direction, and power, certain combinations of bin values may not be observed within the monitoring period, particularly when the monitoring duration is short, resulting in empty bins. Several strategies have been proposed in the literature to address this issue.

330

For instance, Noppe et al. (2020) suggests filling empty bins with the maximum damage value observed in adjacent or neighboring bins, thereby maintaining conservative fatigue estimates. Pacheco et al. (2023) proposes a more sophisticated interpolation approach, fitting a three-dimensional surface to the damage matrix to estimate missing values. Simpler and more commonly applied methods include filling empty bins with the mean damage from samples in the same wind speed bin, the 90th percentile, or the maximum damage. For example, Hübler et al. (2018) suggests filling the empty bins with highest statistical damage value of the same wind speed bin but concludes that in this strategy bins are filled up conservatively leading to reduced

335 lifetimes. However, Hübler and Rolfes (2022) adopts filling empty bins with the maximum value observed in the surrounding bins as suggested by Noppe et al. (2020).

340

In this study, the performance of bins filling with mean, 90th percentile and maximum damage value of the same wind speed bin is evaluated (see Fig. A1, Appendix A). Extreme values—such as the 90th percentile or maximum—tends to significantly overestimate fatigue damage, thus underestimating fatigue life. In contrast, mean-value bin filling yields more consistent and realistic fatigue predictions and is therefore adopted throughout this work.

345

4.1.3 Random Forest Model

Random Forest is an ensemble learning method widely applied to regression and classification tasks. It enhances prediction accuracy and stability by constructing multiple decision trees and aggregating their outputs. Each tree is trained on a bootstrap sample, created by sampling with replacement from the original dataset, and, at each split, a random subset of features is considered to increase model diversity and reduce overfitting risk. RF models demonstrate strong adaptability to high-dimensional and large-scale datasets, as well as robustness in handling missing values, unbalanced data, noise, and outliers. Furthermore,

350

RF inherently provides feature importance rankings, offering valuable insight into the relative contribution of input variables to the prediction outcome (Karadeniz (2025)).

355 The RF regression model is used to predict 10-minutes fatigue damage based on input SCADA and wave parameters. To handle categorical variables, turbine operational states, as described in [Section 3.2](#), are transformed using one-hot encoding, converting each category into a separate binary feature. The target variable, 10-minutes damage, is normalized using a MinMaxScaler to scale values between 0 and 1, facilitating stable model training.

RF model is trained using open source python package Scikit-learn (Pedregosa et al. (2011)) and a bayesian optimization approach is employed for tuning the hyperparameters of the RF model using Hyperopt package in python (Bergstra et al. (2013)). The hyperparameter search space includes the number of estimators (`n_estimators (10, 300)`), maximum depth of trees (`max_depth (2, 15)`), minimum samples required to split a node (`min_samples_split (2, 15)`), and the minimum number of samples required at a leaf node (`min_samples_leaf (1, 7)`).

Bayesian optimization is performed with a maximum of 50 evaluations (`max_evals=50`) to identify the optimal set of hyperparameters. Each monitoring period ΔT_m is split into 80% training and 20% testing subsets to evaluate the model performance and generalizability.

4.2 Statistical uncertainty estimation

Statistical uncertainty in this paper refers to the scatter in fatigue life predictions by models trained using ΔT_m , but the starting point of ΔT_m could be anywhere within $T_{curr} - T_o$ as shown in Fig. 4. This aims to answer the question, how much does the starting point SP of the measurement campaign influence the outcome on T_{EOL} after a campaign of ΔT_m months.

370 To achieve this, the monitoring period ΔT_m is varied from 1 month to 24 months to study the effect of varying data size on the model predictions. For each size of monitoring period ΔT_m , the starting point (SP) ([Figure Fig. 4](#)) is randomly varied to 20 different positions to study the effect of starting point of monitoring data. [To ensure that each monitoring period is fully contained within the available dataset, the start point \(SP\) is restricted such that the monitoring period \$\Delta T_m\$ does not extend beyond \$T_{curr}\$ thus, the latest allowable SP is \$T_{curr} - \Delta T_m\$.](#) This gives 20 different models for each monitoring period ΔT_m as shown in Table 2. An extrapolation model trained with monitoring period ΔT_m and with a random starting point SP is denoted as $M_{\Delta T_m - SP}$. Each model predicts 10-minute fatigue damage which is accumulated to a fatigue life thus giving 20 different predictions for each monitoring period ΔT_m .

4.3 Damage extrapolation for T_{EOL}

Damage extrapolation to estimate T_{EOL} is done by resampling long-term SCADA and wave parameters from $T_{curr} - T_o$, including data from both within and before and after the monitoring window, with replacement to create a synthetic dataset for 20 years, reflecting the full lifetime, which are used to predict fatigue life. Each trained model is used to predict 10-minute damages using this synthetic dataset. The predicted damages are accumulated to get yearly accumulated fatigue damage which is used to calculate mean yearly damage as shown in Fig. 5. Mean yearly damage is calculated using equation 7.

Table 2. Model development for statistical uncertainty estimation using different data sizes and starting points

ΔT_m [Months] → Starting Point [SP] ↓	1	2	3	6	9	12	15	18	21	24
1	M_{1-1}	M_{2-1}								
2	M_{1-2}	M_{2-2}								
...										
20	M_{1-20}	M_{2-20}								

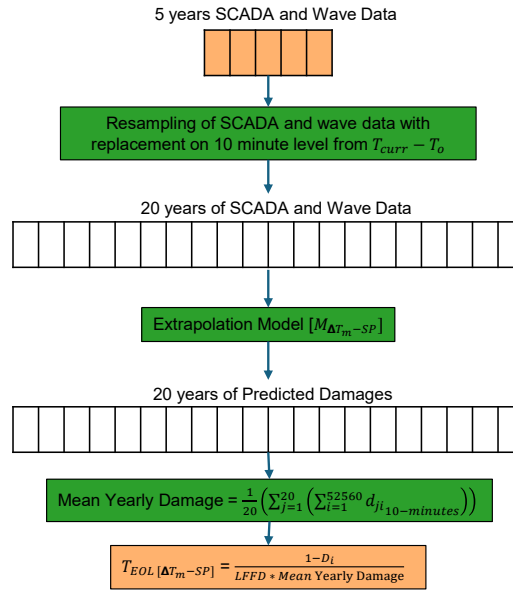


Figure 5. Extrapolation of ~~10-minute~~ 10-minute damages to calculate end of life of OWT

$$\text{Mean Yearly Damage} = \frac{1}{20} \times \left(\sum_{j=1}^{20} \sum_{i=1}^{52560} d_{ji_{(10-minutes)}} \right) \quad (7)$$

385 Where i is the number of ~~10-minute~~ 10-minute samples in each year and j is the total number of years. d_{ji} is the i^{th}
 10-minute fatigue damage for j^{th} year. The resampling of the 5-year monitoring period into a synthetic 20-years dataset is primarily useful when analysing year to year damage variability; however, since this study relies only on the mean yearly damage for estimating T_{EOL} , the choice of using a resampled 20-year period does not affect the results.

390 The mean yearly damage is used to calculate fatigue life T_{EOL} as shown in Fig. 5. The fatigue life T_{EOL} is calculated using equation 8.

$$T_{\text{EOL}} [\Delta T_m - \text{SP}] = \frac{1 - D_i}{LFFD_{\text{factor}} \times \text{Mean Yearly Damage}} \quad (8)$$

D_i is the initial damage including but not limited to pile driving damage, transportation damage, fatigue damage of the monopile foundations before start of normal operation, before turbine mounting and powering. In this study D_i is considered as zero as it does not affect the [models-model](#) comparison. In line with findings in Sadeghi et al. (2023a) a low frequency fatigue factor $LFFD_{\text{factor}}$ can be included to account for long term cycles, that don't close within the default ~~10-minute~~ [10-minute](#) window, however for simplicity a ~~LFFD=1~~ [LFFD=1](#) is used.

5 Results

This section presents a comparative evaluation of the binning approach with varying dimensionality and Random Forest models across different target variables—namely, single-sensor, FA, and SS damage. The predicted fatigue life for single sensor and FA is normalized between (0.1–1) using Equation 9. The scaling of SS fatigue lifetimes is done with the same scale as of FA fatigue life to retain their relative magnitudes for comparison.

$$\bar{T}_{\text{EOL}} = \left(\frac{T_{\text{EOL}} - T_{\text{EOL},\text{min}}}{T_{\text{EOL},\text{max}} - T_{\text{EOL},\text{min}}} \right) \times (\text{Scale}_{\text{max}} - \text{Scale}_{\text{min}}) + \text{Scale}_{\text{min}} \quad (9)$$

where:

- T_{EOL} is the predicted fatigue life,
- \bar{T}_{EOL} is the scaled fatigue life,
- $T_{\text{EOL},\text{min}}$ and $T_{\text{EOL},\text{max}}$ are the minimum and maximum predicted fatigue life values [across all months obtained from all extrapolation approaches, across all dataset sizes and randomly selected start points](#),
- $\text{Scale}_{\text{min}} = 0.1$ and $\text{Scale}_{\text{max}} = 1$ define the target range for scaled fatigue life suitable for plotting on log-axis.

5.1 Feature selection

Feature selection was initially performed using a filter-based method that identifies the top five features for each target variable. These selected features are summarized in Table 3. The numbers in Table 3 refer to the relative importance of the selected features with 1 being most important feature.

For the 3 MW OWT, the results suggest a dominant influence of SCADA parameters across most target variables, with the exception of SS direction, which shows a dependency on mean wave height. In contrast, the 9 MW OWT displays a greater sensitivity to wave-related parameters across all target variables, reflecting the increased susceptibility of larger monopile structures to wave-induced effects as already mentioned by Velarde et al. (2020); Wu et al. (2025). Notably, the SS direction

Table 3. Overview of selected features for different target variable for 3MW and 9MW OWT

Variable	3MW OWT			9MW OWT		
	Single sensor 205°	Fore-Aft	Side-Side	Single sensor 230°	Fore-Aft	Side-Side
Windspeed <u>Wind speed</u>	5	3	1	5	3	
Yaw Angle	1			2		2
Pitch Angle	3	2	4	1	2	
Power	2	5	5			
Rotational Speed		1			4	
Turbulence Intensity	4	4	2	4	1	
Operational State*	✓	✓	✓	✓	✓	✓
Mean Wave Height			3	3	5	1
Mean Wave Period						4
High Frequent Wave Direction						5
Low Frequent Wave Direction						
Tidal level						3

* Operational state is deliberately included in all models (a 5D model contains 5-EOC parameters and turbine operational state)

for the 9 MW OWT incorporates all wave parameters except low-frequency wave direction. While wind speed and turbulence intensity are commonly used for fatigue estimation (as studied by Noppe et al. (2020) on 2MW OWT), our feature selection approach identifies variables that provide the greatest incremental predictive value for each target. Turbulence intensity is selected for most targets, and wind speed is included in all binning strategies (except for side-side direction of 9 MW OWT), ensuring that standard fatigue predictors are considered alongside additional influential features. Some of the selected features exhibit correlations. Random Forest feature importance evaluates each variable's contribution to reducing node impurity across all trees, so correlated variables can still be selected if they provide incremental predictive information (Breiman (2001)). The top five features are thus those with the highest combined predictive relevance, and their selection reflects the overall importance rather than strict independence. Future work could explore dimensionality reduction methods to explicitly account for feature correlation.

In addition to the filter-based approach, RFECV was applied both globally, RFECV-Global, and separately within each turbine operational state, RFECV-Statewise. The results of these RFECV-based feature selection strategies are provided in Appendix B.

5.2 Single Sensor

The fatigue damage predictions from both binning and RF models vary depending on the size of the monitoring dataset and the starting point of the data used for training. Figure 6 presents a comparison of fatigue life predictions obtained using binning (from 1D to 5D) and a 5D RF model for a 3 MW OWT.

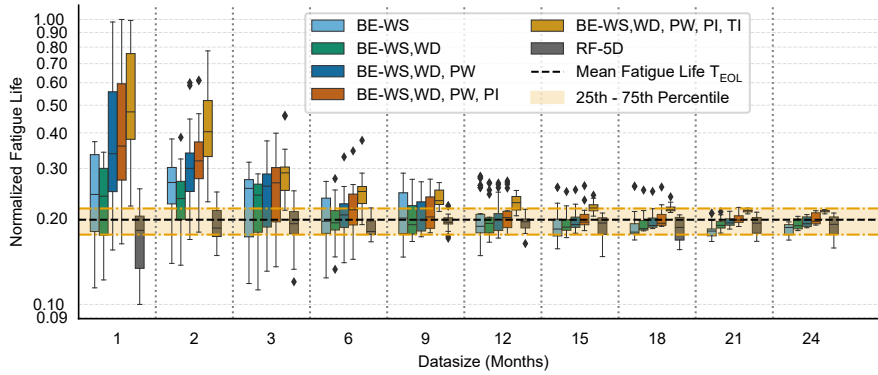


Figure 6. Comparison of binning (1D to 5D) and 5D random forest model for a 3MW OWT at 205° single sensor

The mean fatigue life T_{EOL} denoted by grey dotted line in Fig. 6 represents the true value of fatigue life calculated using
 435 actual measurement data. The 25th–75th percentile between dotted orange lines is calculated by resampling the full monitoring
 period with replacement to synthetically generate 100 years of data. Fatigue life is then calculated for each synthetic year to
 get a distribution, with mean and percentiles plotted in Fig. 6. The uncertainty bounds shown in Fig. 6 represent the variability
 in fatigue life estimates obtained from linear extrapolation (0-D binning) across multiple individual 1 year periods, rather than
 uncertainty across multiple 20-year spans. When multiple synthetic 20-year periods are generated, the resulting fatigue-life
 440 estimates show minimal spread and converge to the Mean Fatigue Life T_{EOL} line in Fig. 6.

Across all extrapolation models, a general reduction in prediction scatter is observed as the monitoring period increases
 confirming the conclusions of Pacheco et al. (2023) stating that the uncertainties in extrapolations decrease with increasing
 monitoring period. Notably, the prediction variability in binning approaches decreases with higher binning dimensions (e.g.,
 from 1D to 5D). However, higher-dimensional binning tends to over-predict fatigue life, primarily due to the presence of empty
 445 bins. This sensitivity to the bin-filling strategy highlights a limitation of binning with limited data availability.

In contrast, the RF models consistently show lower scatter in predictions for smaller data sizes of 6–9 months. As data
 availability increases, predictions from all models begin to converge, ~~with comparable performance across methods.~~ Higher
 dimensional binning, particularly 5D binning, provides consistently lower scatter in predictions from 9 months onwards, but
 the mean values of predictions are shifted because of unoptimized bin sizing and bin filling strategy. The RF-5D model shows
 450 higher uncertainty and is outperformed by the binning approaches for data sizes ~~beyond greater than~~ 18 months.

Figure 7 shows similar trends for the 9 MW OWT. Higher-dimensional binning again suffers from the presence of empty
 bins and heightened sensitivity to the bin-filling strategy, especially at smaller data sizes. The RF model demonstrates superior
 performance with significantly lower scatter in predictions for data sizes up to 9 months. While the difference in prediction
 variability between RF and binning models diminishes for larger data sizes of 18–21 months, the higher-dimensional binning
 455 methods still tend to overestimate fatigue life.

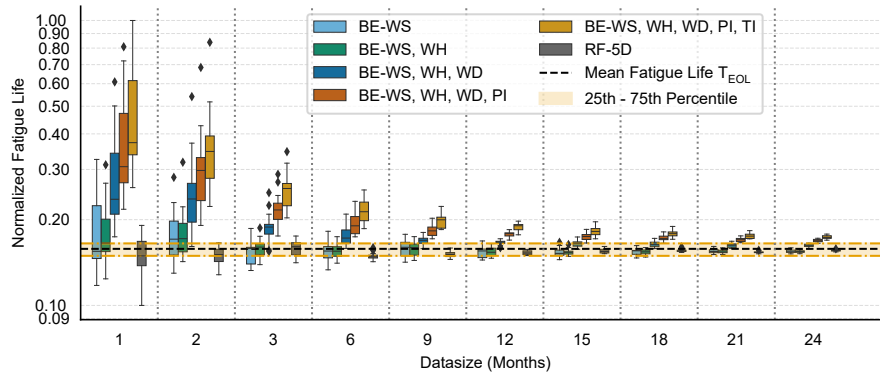


Figure 7. Comparison of binning (1D to 5D) and 5D random forest model for a 9MW OWT at 230° single sensor

A comparison of various RF model configurations including feature sets selected using RFECV on global data, RFECV applied separately to each operational state, and models trained using all available features is provided in Fig. C1 and C2 in Appendix C for both 3 MW and 9 MW OWTs. The results suggest that using statewide RFECV and individual models per operational state slightly reduces prediction scatter but introduces additional model complexity.

460 Figure 8 illustrates the variability in predicted damage across different data sizes and starting points, binned by wind speed intervals, for 1D binning and RF models applied to a 3 MW OWT. As shown in Fig. 8, the mean predicted damage stabilizes after approximately 9–12 months of monitoring data for both the binning and RF models. However, the interquartile range (IQR), representing the spread in predictions, is consistently narrower and converges more rapidly for the RF model, indicating greater robustness to variability in starting point. ~~Notably, higher IQR values persist~~ As shown in Fig. 8 (right), the IQR in the wind
 465 speed bin [21.0, 22.0) even after 12 is consistently higher for the RF model than for the binning approach once more than 15
months of data, which can be attributed to the low occurrence frequency of this wind speed range, leading to reduced statistical
confidence are available. This increased scatter reflects the limited data availability in high-wind conditions. Consequently, for
data sizes beyond approximately 15 months, the RF-5D model is outperformed by the binning-based approach, consistent with
the trends observed in Fig. 6.

470 Similar trends are observed in the damage predictions for the 9 MW OWT, as illustrated in Fig. 9. For the wind speed bin [7.0, 8.0), the IQR of the RF model predictions converges after approximately 9 months of data. In contrast, the IQR for the binning approach continues to decrease gradually with increasing data size, indicating a slower convergence. ~~For the higher~~ As
shown in Fig. 9 (right), the IQR in the wind speed bin [25.0, 26.0), both RF and binning approaches exhibit minor fluctuations
in IQR beyond 9 fluctuates between the RF-5D model and the binning approach across different data sizes. For 6, 12, and
 475 18 months of data. However, the magnitude of these fluctuations remains relatively low, the binning IQR is lower, whereas
for 9 and 15 months, the RF-5D model exhibits slightly lower variability. These minor shifts arise from the very limited data
available in this high wind speed bin, where low occurrence probability causes this apparent variability.

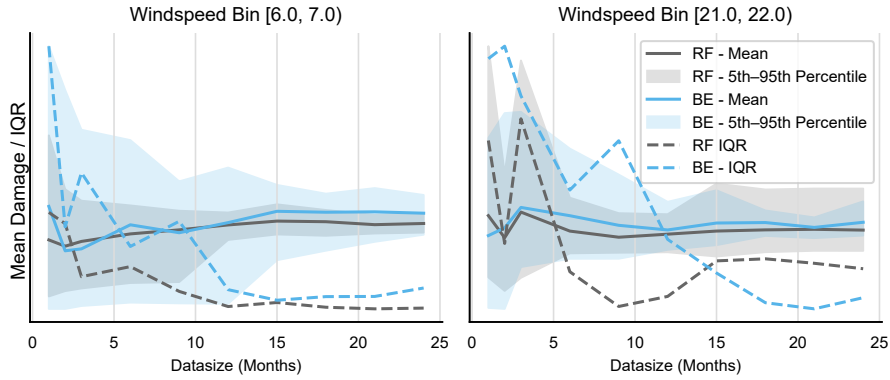


Figure 8. Mean and IQR of predicted damages using 1D-binning and 5D-RF model in windpeed bin of [6.0,7.0)-left and [21.0,22.0)-right for a 3MW OWT-single sensor

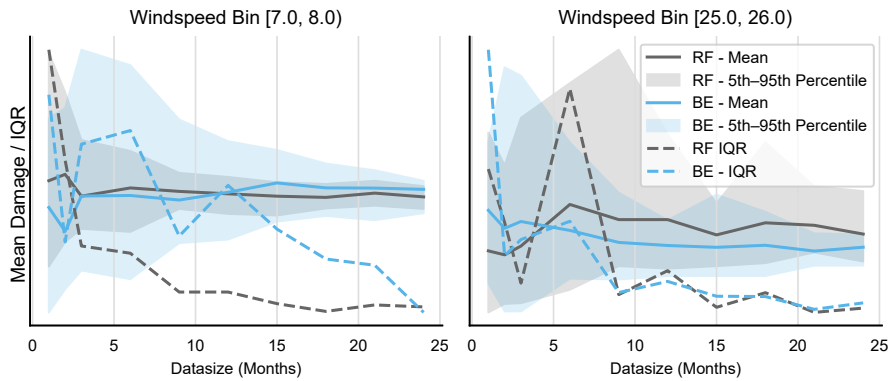


Figure 9. Mean and IQR of predicted damages using 1D-binning and 5D-RF model in windpeed bin of [7.0,8.0)-left and [25.0,26.0)-right for a 9MW OWT-single sensor

5.3 Fore-Aft direction

Figure 10 presents the comparison of fatigue life predictions in the FA direction for the 3 MW OWT. The RF models exhibit a relatively constant scatter in predictions beyond 9 months of training data. For smaller data sizes of 6–9 months, RF models outperform binning methods showing lower scatter. However, for larger data sizes of greater than 12 months, higher-dimensional binning models, particularly 2D and 3D, show reduced scatter compared to RF models, indicating improved performance in fatigue life estimation.

The variability in RF predictions is further minimized by incorporating additional features, either through RFECV or by training separate RF models for each turbine operational state. The results for these alternative RF configurations are provided in Fig. C3 and C4 in Appendix C.

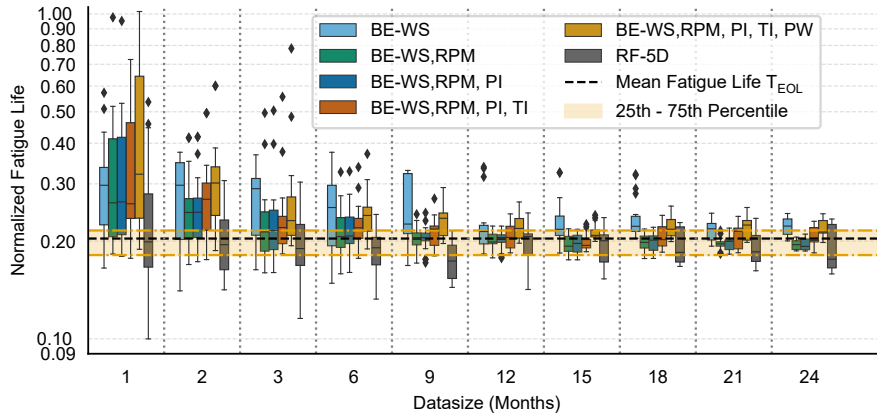


Figure 10. Comparison of binning (1D to 5D) and 5D random forest model for a 3MW OWT in Fore-Aft direction

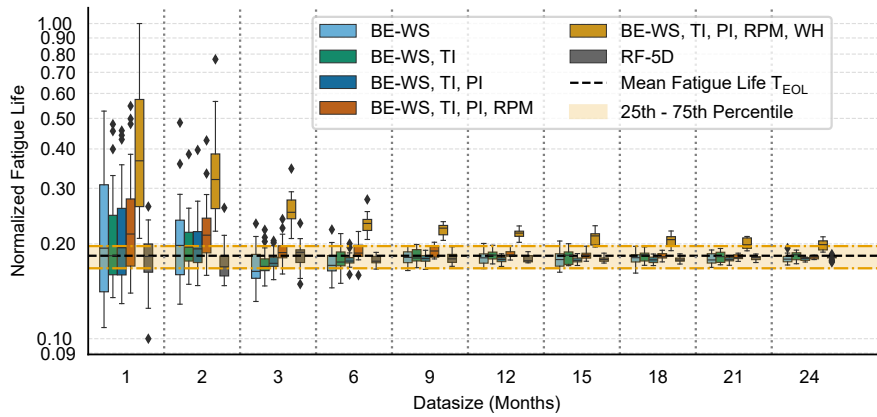


Figure 11. Comparison of binning (1D to 5D) and 5D random forest model for a 9MW OWT in Fore-Aft direction

A similar comparison for the 9 MW OWT is illustrated in Fig. 11. In this case, RF models demonstrate superior performance at smaller data sizes, while all extrapolation methods converge to similar prediction accuracy as the data size increases. Looking at 3 months predictions in Fig. 11, it can be noted that the predictions even for 4D binning are almost within the target region showing lesser influence of empty bins for the 9 MW OWT in FA direction, except in the case of 5D binning, which tends to overestimate fatigue life even when larger data sizes are used.

5.4 Side-Side direction

Figure 12 illustrates the trends in fatigue life predictions for SS direction in the 3 MW OWT. Similar to the single sensor and FA direction cases, RF models exhibit reduced scatter at smaller data sizes of 6–9 months, and all models—including binning and RF—converge to comparable performance as the data size increases.

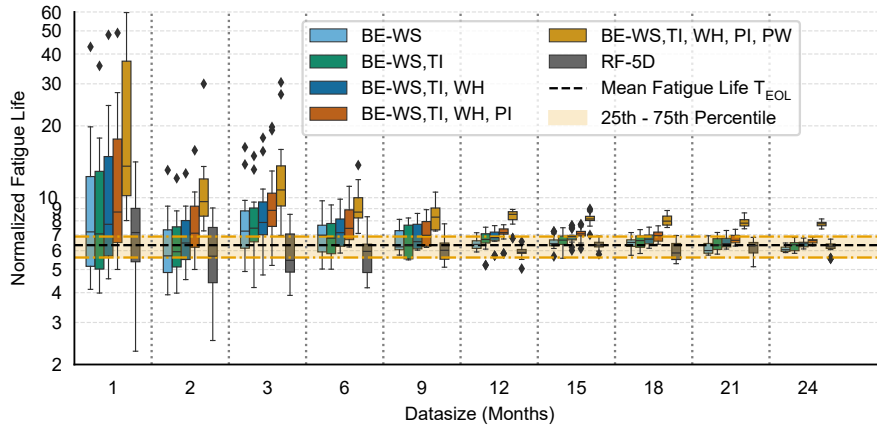


Figure 12. Comparison of binning (1D to 5D) and 5D random forest model for a 3MW OWT in Side-Side direction

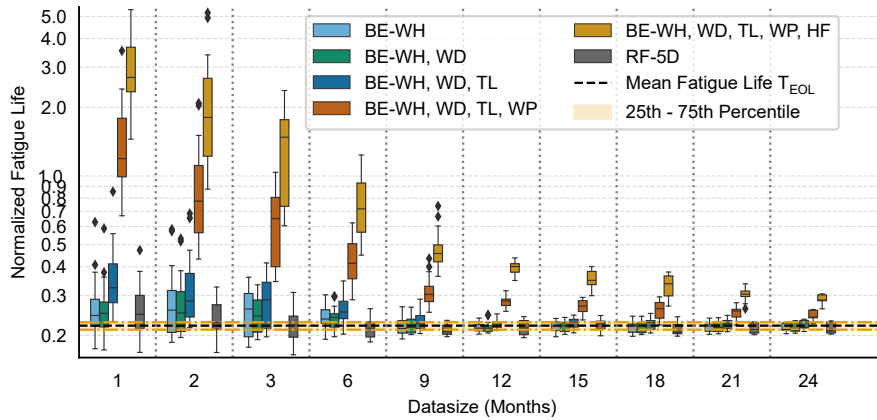


Figure 13. Comparison of binning (1D to 5D) and 5D random forest model for a 9MW OWT in Side-Side direction

For the 9 MW OWT, SS direction predictions show noticeable differences across models, as depicted in Fig. 13. Higher-dimensional binning approaches struggle to provide reliable predictions due to the increased sensitivity to empty bins and data sparsity. In contrast, ~~RF models maintain consistent and reasonable~~ both lower dimensional binning (1D and 2D) and RF models show consistent and comparable performance, particularly ~~at smaller data sizes of~~ for data sizes greater than 6 -9 500 months.

Notably, no significant improvement in SS direction predictions was observed through the inclusion of additional features, nor by employing RFECV or statewise RF modeling strategies, as summarized in Fig. C5 and C6 in Appendix C.

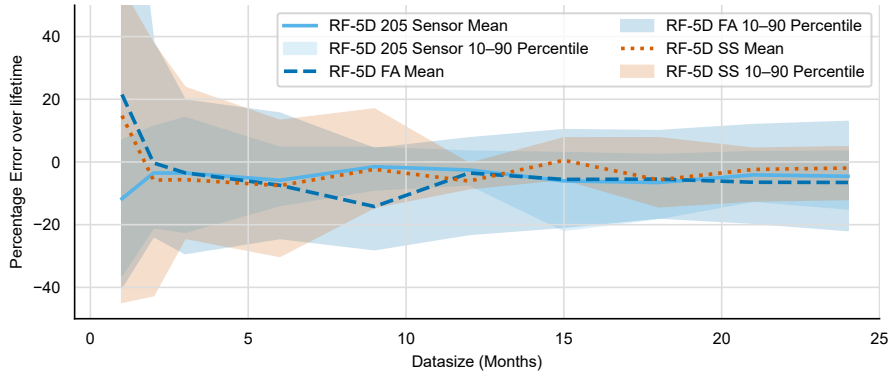


Figure 14. Percentage errors in lifetime estimation for random forest models with single sensor, FA and SS directions for 3MW OWT

5.5 Prediction performance for different target parameters

The percentage errors over lifetime are defined as given in equation 10, where $T_{\text{EOL, mean}}$ is the mean fatigue life calculated using actual measurement data as described in section 5.2 and T_{EOL} are the predicted values of fatigue life.

$$\text{Percentage Error over Lifetime} = \left(\frac{T_{\text{EOL}} - T_{\text{EOL, mean}}}{T_{\text{EOL, mean}}} \right) \times 100 \quad (10)$$

The percentage errors over lifetime in fatigue life predictions for different target variables, FA, SS and single sensor, associated with varying training data sizes and starting points are presented in Fig. 14 for the 3 MW OWT. For both FA and single sensor targets, the 10 – 90th percentile of the prediction errors stabilizes after approximately 9 months of training data. In contrast, predictions for the SS direction exhibit continued variability, the 10 – 90th percentile of the prediction errors shows a notably low value at 12 months. Considering the low value at 12 months a statistical outlier, the SS prediction errors also stabilize after approximately 9 months of data size. With 12 months of data, the FA direction yields prediction errors in the range of $[-22\%, +8\%]$, while single sensor predictions remain within a narrower error margin of approximately $\pm 5\%$. SS predictions at 12 months show improved accuracy with errors in the range of $[-8\%, 0\%]$, but the error increases to $[-21\%, +7\%]$ at 15 months before decreasing again with larger data sizes.

Figure 15 shows a similar trend for the 9 MW OWT, where error convergence is observed for all three directions, single sensor, FA, and SS. The overall prediction errors for the 9 MW OWT are lower compared to the 3 MW turbine. Specifically, using 12 months of training data, the RF model predicts lifetime errors for the single sensor target within $[-10\%, -2\%]$, for the FA direction within $[-7\%, +2\%]$, and for the SS direction within approximately $\pm 18\%$.

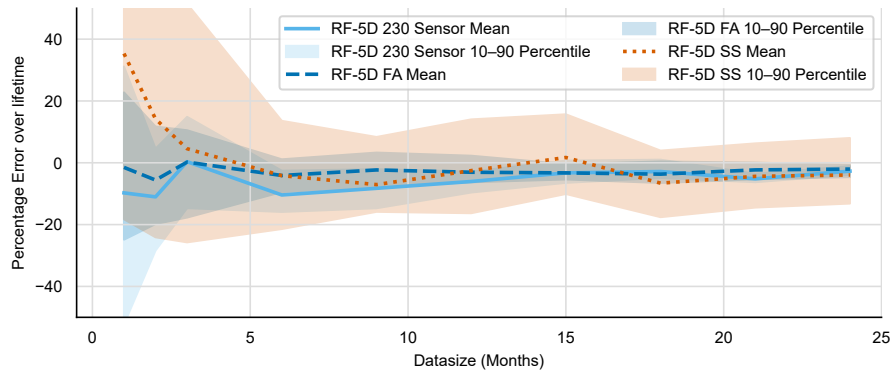


Figure 15. Percentage errors in lifetime estimation for random forest models with single sensor, FA and SS directions for 9MW OWT

520 6 Discussions

The features selected through the filter-based feature selection method highlight the greater importance of wave parameters for SS direction in both 3 MW and 9 MW OWTs. Furthermore, the larger 9 MW turbine appears more sensitive to wave-induced fatigue loading compared to the smaller 3 MW turbine.

Analysis of the variation in mean damage values across different wind speed bins for the 3 MW and 9 MW turbines with increasing data sizes indicates that predictions converge after approximately 9–12 months of monitoring data. Additionally, the scatter in predictions is significantly lower for RF models than for binning-based extrapolation for smaller data sizes. For larger data sizes, for example, in the 3 MW OWT case beyond 18 months, the RF models show comparable or higher scatter and are outperformed by binning-based extrapolation models. A strain monitoring period of 9-10 months is also recommended in the literature (Hübler et al. (2018); Hübler and Rolfes (2022)) to capture critical fatigue-inducing events, such as high wind speeds and seasonal variability, provided that no significant changes occur in the turbine or its EOCs during this time.

The availability of long-term monitoring data enables the investigation of how the randomly varying starting point of the monitoring period affects-influences the variability in fatigue life estimates. A comprehensive comparison between binning and RF model predictions shows that when accurate fatigue life estimates are required in shorter timeframes of 6-9 months, RF models yield lower statistical uncertainty than binning approaches. RF models are more effective at capturing the nonlinear relationships between SCADA and wave parameters and fatigue damage, particularly when limited data is available. For longer data durations, greater than 15 months, both RF and binning methods provide comparable fatigue life predictions. When long term measurements data is available, binning extrapolation should be preferred as they are more transparent, provide easy control of conservativeness using alternate bin filling strategies and have a stronger link with design as indicated by their similarity to design load cases (DLCs) (IEC (2019); Freudenreich and Argyriadis (2007)).

Increased dimensionality in binning, specially 4D and 5D, results in reduced performance compared to lower-dimensional, 1D and 2D, binning. This is primarily due to the treatment of empty bins. Alternative strategies for empty bin filling, such as using the 90th percentile, the highest neighboring value, or interpolation methods based on surface fitting (Pacheco et al.

(2023); Noppe et al. (2020); Hübler and Rolfes (2022)), could enhance the accuracy of high-dimensional binning. In this study, bin sizes are not explicitly optimized. Future work may involve optimizing bin sizes for different data sizes, similar to
545 hyperparameter tuning in RF models, to further improve binning performance.

From a usability perspective, 1D and 2D binning are computationally efficient and easy to implement. However, higher-dimensional binning, 3D and above, becomes increasingly computationally expensive, especially when combined with complex empty-bin filling strategies. On the other hand, RF models, while offering improved prediction accuracy, are more complex and require intensive hyperparameter tuning. More advanced RF pipelines, such as those involving different models for different
550 operational states, can further enhance accuracy but at the cost of increased computational effort and reduced interpretability.

RF models using filter-based feature selection offer a good trade-off between complexity and predictive performance. In practical scenarios where a turbine is instrumented later in its lifetime and a fast, reliable fatigue life estimate is required, RF models can be particularly valuable.

While this study evaluates the statistical uncertainty associated with varying the start of the monitoring period, another
555 layer of uncertainty arises when predictions are made using a fixed data size and start point, especially if the training and extrapolation data differ significantly. Both binning and RF models in this work rely on the mean damage within each bin or the mean prediction, without considering the full distribution. Such uncertainties have been explored in the context of binning by Sadeghi et al. (2024). Future work could explore the use of Quantile Random Forests (Rouholahnejad and Gottschall (2025b)) to quantify this uncertainty. Additionally, Bayesian neural networks may be employed to flag outliers in fatigue life predictions
560 based on differences between training and extrapolation datasets. These advanced uncertainty quantification techniques are beyond the scope of this paper and are proposed as future work.

Finally, it is important to note that the findings of this study are applicable to the wind farms analyzed and, by extension, are likely relevant to the majority of farms located in the North Sea. However, in locations exhibiting differing levels of environmental variability, the applicability of these recommendations may be limited.

565 7 Conclusions

This study concludes that a monitoring period of 9–12 months is required to obtain reliable fatigue life estimates for OWTs, based on case studies using long-term monitoring data from both 3 MW and 9 MW turbines. Feature selection results further demonstrate that the relevance of input parameters depends on the target variable, i.e., single sensor, FA, or SS damage. For the larger 9 MW OWT, wave parameters appear consistently across all target variables, whereas for the smaller 3 MW turbine, only
570 SS fatigue damage includes mean wave height as a key feature. These conclusions specifically apply to offshore wind farms analyzed within the Belgian North Sea, and requires re-evaluation for locations exhibiting varying degrees of environmental variability.

Random forest models exhibit better generalization capability compared to binning-based extrapolation methods, as evidenced by their reduced sensitivity to the starting point of the monitoring period. ~~While 2D binning outperforms 1D binning,~~
575 ~~higher-dimensional binning,~~ Higher-dimensional binning, 3D and above, suffers from issues with empty bins, especially when

using smaller datasets. Consequently, RF models are more effective for fatigue life prediction when limited data is available, offering lower statistical uncertainty than binning methods.

The predictive advantage of RF models over binning diminishes as the monitoring period increases, beyond 12-15 months, at which point both approaches yield comparable performance. Furthermore, more complex RF models involving additional features or operational state-specific modeling offer only marginal improvements in accuracy.

Future work may enhance the accuracy of binning methods by optimizing bin sizes and systematically evaluating the effects of various empty bin filling strategies. These improvements could help narrow the performance gap between binning and machine learning-based approaches, particularly for high-dimensional binning models.

Data availability. The data used in this paper is proprietary to the industrial partners of this project and cannot be made publicly available

585 Appendix A: Effect of different bin filling strategies using 3D binning

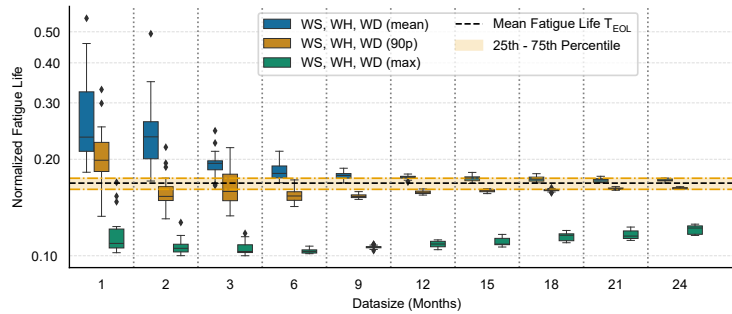


Figure A1. Effect of different bin filling strategies on lifetime predictions using 3D binning for a 9MW OWT at 230° single sensor

Appendix B: Feature selection using RFECV-Global and Statewise

B1 RFECV-Global features

RFECV was applied to 12 months of data to identify the most relevant features for fatigue life prediction. Operational states were incorporated into the feature space using one-hot encoding. The selected features for both the 3 MW and 9 MW offshore wind turbines are given in Table B1.

Table B1. Selected features for different target variable for 3MW and 9MW OWT using RFECV on 12 months of data

Variable	3MW OWT			9MW OWT		
	Single sensor 205°	Fore-Aft	Side-Side	Single sensor 230°	Fore-Aft	Side-Side
Windspeed <u>Wind speed</u>	✓	✓	✓		✓	✓
Yaw Angle	✓		✓	✓	✓	✓
Pitch Angle	✓	✓	✓	✓	✓	
Power	✓	✓	✓	✓	✓	
Rotational Speed	✓	✓	✓	✓	✓	
Turbulence Intensity	✓	✓	✓	✓	✓	✓
Operational State*	✓	✓	✓	✓	✓	✓
Mean Wave Height	✓	✓	✓	✓	✓	✓
Mean Wave Period			✓		✓	✓
High Frequent Wave Direction	✓		✓			✓
Low Frequent Wave Direction			✓			✓
Tidal level			✓			✓

* Operational state is deliberately included in all models

B2 RFECV-Statewise features

RFECV was applied to 12 months of data by first filtering the dataset into individual operational states and performing RFECV separately on each subset. The resulting RFECV-Statewise feature sets for both the 3 MW and 9 MW offshore wind turbines are given in Table B2 and B3.

595 Appendix C: Comparison of different RF configurations

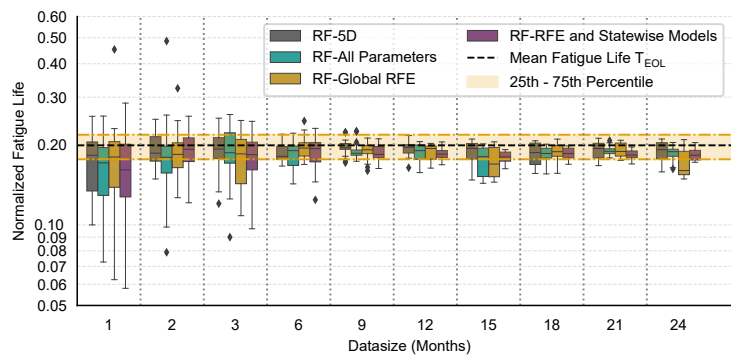


Figure C1. Comparison of different RF model configurations for a 3MW OWT at 205° single sensor

Table B2. Operational state-wise selected features using RFECV-Statewise on 12 months of data for 3MW

Operational State → Parameters ↓	Single sensor 205°				Fore-Aft				Side-Side			
	1	2	3	4	1	2	3	4	1	2	3	4
Windspeed <u>Wind speed</u>	✓	✓	✓	✓	✓	✓	✓	✓	✓	✓	✓	✓
Yaw Angle	✓	✓	✓	✓	✓	✓	✓	✓	✓	✓	✓	
Pitch Angle	✓	✓		✓	✓	✓		✓	✓			
Power	✓		✓	✓	✓	✓	✓	✓	✓	✓	✓	
Rotational Speed	✓		✓	✓	✓	✓	✓	✓		✓	✓	
Turbulence Intensity	✓		✓	✓	✓	✓	✓	✓	✓	✓	✓	✓
Operational State*	✓	✓	✓	✓	✓	✓	✓	✓	✓	✓	✓	✓
Mean Wave Height	✓	✓	✓	✓	✓	✓	✓	✓	✓	✓	✓	✓
Mean Wave Period		✓	✓	✓		✓	✓	✓	✓	✓	✓	
High Frequent Wave Direction	✓	✓	✓	✓		✓	✓	✓		✓	✓	✓
Low Frequent Wave Direction	✓	✓	✓	✓	✓	✓	✓	✓	✓	✓	✓	
Tidal level		✓	✓	✓		✓	✓	✓	✓	✓	✓	✓

1: Nominal, 2: Idling, 3: Highwind, 4: Invalid

* Operational state is deliberately included in all models

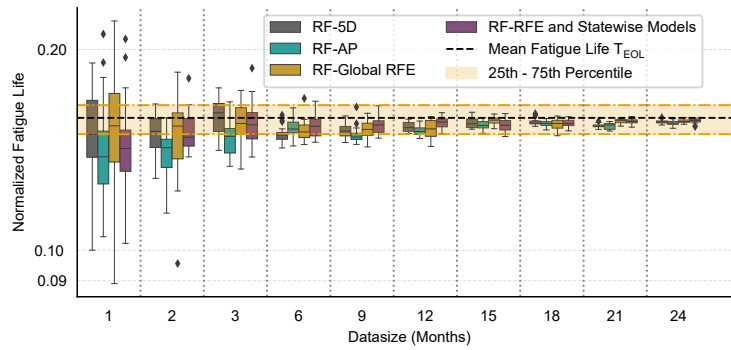


Figure C2. Comparison of different RF model configurations for a 9MW OWT at 230° single sensor

Table B3. Operational state-wise selected features using RFECV-Statewise on 12 months of data for 9MW

Operational State → Parameters ↓	Single sensor 230°				Fore-Aft				Side-Side			
	1	2	3	4	1	2	3	4	1	2	3	4
Windspeed <u>Wind speed</u>	✓	✓	✓	✓	✓	✓	✓	✓	✓	✓		✓
Yaw Angle	✓		✓		✓		✓		✓	✓	✓	
Pitch Angle	✓		✓	✓	✓		✓	✓		✓		✓
Power	✓		✓	✓	✓		✓	✓	✓	✓		✓
Rotational Speed	✓		✓	✓	✓	✓	✓	✓	✓			✓
Turbulence Intensity	✓		✓	✓	✓		✓	✓	✓	✓	✓	✓
Operational State*	✓	✓	✓	✓	✓	✓	✓	✓	✓	✓	✓	✓
Mean Wave Height	✓	✓	✓	✓	✓	✓	✓	✓	✓	✓	✓	✓
Mean Wave Period	✓		✓	✓	✓		✓	✓	✓	✓	✓	✓
High Frequent Wave Direction	✓		✓				✓	✓	✓	✓	✓	✓
Low Frequent Wave Direction			✓	✓			✓	✓	✓	✓	✓	✓
Tidal level	✓		✓	✓	✓		✓	✓	✓	✓	✓	✓

1: Nominal, 2: Idling, 3: Curtailed, 4: Invalid

* Operational state is deliberately included in all models

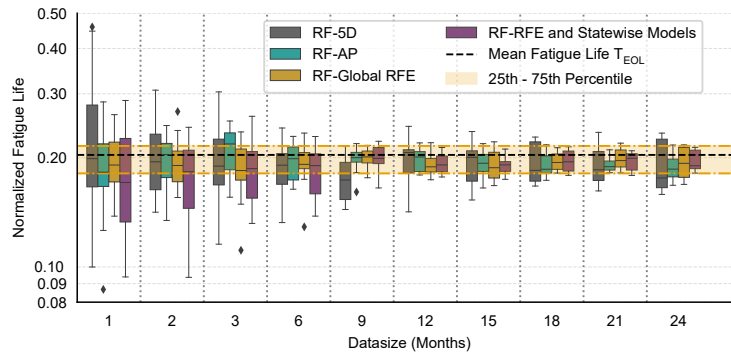


Figure C3. Comparison of different RF model configurations for a 3MW OWT in FA direction

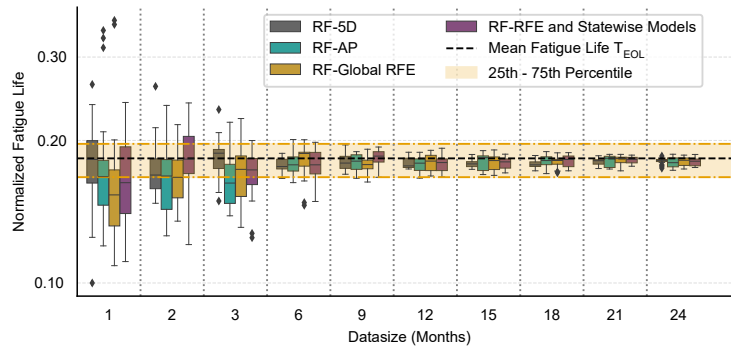


Figure C4. Comparison of different RF model configurations for a 9MW OWT in FA direction

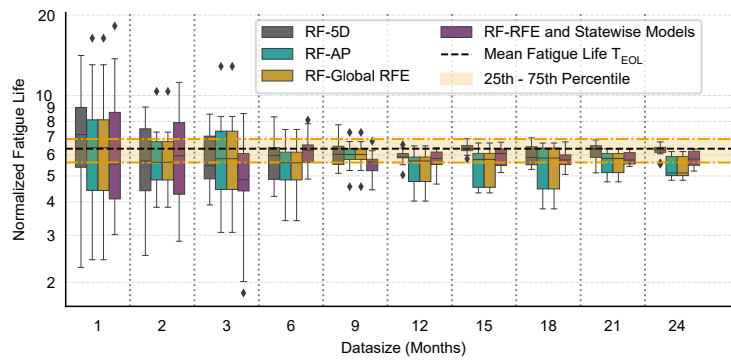


Figure C5. Comparison of different RF model configurations for a 3MW OWT in SS direction

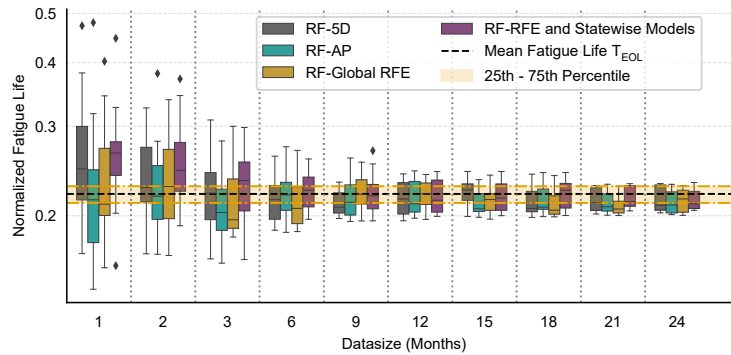


Figure C6. Comparison of different RF model configurations for a 9MW OWT in SS direction

Table D1. Bin sizes for SCADA and wave parameters

<u>Variable</u>	<u>Wind speed</u>	<u>Yaw Angle</u>	<u>Pitch Angle</u>	<u>Power</u>	<u>Rotational Speed</u>	<u>Turbulence Intensity</u>	<u>Mean Wave Height</u>	<u>Mean Wave Period</u>	<u>High Frequency Wave Direction</u>	<u>Low Frequency Wave Direction</u>	<u>Tidal Level</u>
<u>Units</u>	<u>m/s</u>	<u>°</u>	<u>°</u>	<u>kW</u>	<u>rpm</u>	<u>%</u>	<u>cm</u>	<u>s</u>	<u>°</u>	<u>°</u>	<u>cm</u>
<u>Bin Size</u>	<u>1</u>	<u>10</u>	<u>5</u>	<u>250</u>	<u>0.5</u>	<u>5</u>	<u>10</u>	<u>0.2</u>	<u>10</u>	<u>10</u>	<u>10</u>

Appendix D: Bin sizes

Author contributions. AM: conceptualizing, analyzing, interpretation, writing. WW: conceptualizing, validation, interpretation, supervision. NS: interpretation, validation. CD: supervision, data collection, validation. All authors contributed to the review and editing.

Competing interests. The authors have no competing interests.

600 *Disclaimer.* TEXT

Acknowledgements. We acknowledge Parkwind and Norther for their permission to use the monitoring data. We acknowledge the support of VLAIO through De Blauwe Cluster cSBO FIRMEST project. We acknowledge WILLOW project, funded by the European Union with GA No. 101122184. Views and opinions expressed are however those of the author(s) only and do not necessarily reflect those of the European Union. Neither the European Union nor the granting authority can be held responsible for them.

605 During the preparation of this work, the author(s) used ChatGPT5 to improve the text. After using this tool/service, the author(s) reviewed and edited the content as needed and take(s) full responsibility for the content of the publication.

References

- BASQUIN, O.: The exponential law of endurance tests, in: Proc am soc test mater, vol. 10, pp. 625–630, 1910.
- Bergstra, J., Yamins, D., and Cox, D.: Making a Science of Model Search: Hyperparameter Optimization in Hundreds of Dimensions for
610 Vision Architectures, in: Proceedings of the 30th International Conference on Machine Learning, edited by Dasgupta, S. and McAllester, D., vol. 28 of *Proceedings of Machine Learning Research*, pp. 115–123, PMLR, Atlanta, Georgia, USA, <https://proceedings.mlr.press/v28/bergstra13.html>, 2013.
- Bezziccheri, M., Castellini, P., Evangelisti, P., Santolini, C., and Paone, N.: Measurement of mechanical loads in large wind turbines: Problems on calibration of strain gage bridges and analysis of uncertainty, *Wind Energy*, 20, 1997–2010,
615 <https://doi.org/https://doi.org/10.1002/we.2136>, 2017.
- Bossanyi, E.: Surrogate model for fast simulation of turbine loads in wind farms, *Journal of Physics: Conference Series*, 2265, 042 038, <https://doi.org/10.1088/1742-6596/2265/4/042038>, 2022.
- Bouty, C., Schafhirt, S., Ziegler, L., and Muskulus, M.: Lifetime extension for large offshore wind farms: Is it enough to reassess fatigue for selected design positions?, *Energy Procedia*, 137, 523–530, <https://doi.org/https://doi.org/10.1016/j.egypro.2017.10.381>, 14th Deep Sea
620 Offshore Wind RD Conference, EERA DeepWind'2017, 2017.
- Breiman, L.: Random forests, *Machine learning*, 45, 5–32, 2001.
- Breiman, L.: Manual on setting up, using, and understanding random forests, Berkeley: Statistics Department University of California Berkeley, 2002.
- Buljan, A.: 25-Year-Old Danish Offshore Wind Farm Gets Approval to Operate for 25 More Years — offshorewind.biz, <https://www.offshorewind.biz/2025/06/27/25-year-old-danish-offshore-wind-farm-gets-approval-to-operate-for-25-more-years/>, [Accessed 14-07-
625 2025], 2025.
- D'Antuono, P., Weijtjens, W., and Devriendt, C.: OWI-Lab/py_fatigue: Zenodo registration, <https://doi.org/10.5281/zenodo.7656681>, 2023.
- de N Santos, F., D'Antuono, P., Robbelein, K., Noppe, N., Weijtjens, W., and Devriendt, C.: Long-term fatigue estimation on offshore wind turbines interface loads through loss function physics-guided learning of neural networks, *Renewable Energy*, 205, 461–474,
630 <https://doi.org/https://doi.org/10.1016/j.renene.2023.01.093>, 2023.
- de N Santos, F., Noppe, N., Weijtjens, W., and Devriendt, C.: Farm-wide interface fatigue loads estimation: A data-driven approach based on accelerometers, *Wind Energy*, 27, 321–340, 2024.
- DNV-RP-C203: Fatigue design of offshore steel structures, accessed: 2025-07-15, <https://www.dnv.com/energy/standards-guidelines/dnv-rp-c203-fatigue-design-of-offshore-steel-structures/>, 2024.
- 635 DNV-ST-0262: Lifetime extension of wind turbines, accessed: 2024-08-13, <https://www.dnv.com/energy/standards-guidelines/dnv-st-0262-lifetime-extension-of-wind-turbines/>, 2016.
- Fallais, D., Sastre Jurado, C., Weijtjens, W., and Devriendt, C.: Long-term validation of a model-based virtual sensing method for fatigue monitoring of offshore wind turbine support structures: Comparing as-designed with state-of-the-art foundation models, *Marine Structures*, 104, 103 841, <https://doi.org/https://doi.org/10.1016/j.marstruc.2025.103841>, 2025.
- 640 Freudenreich, K. and Argyriadis, K.: The Load Level of Modern Wind Turbines according to IEC 61400-1, *Journal of Physics: Conference Series*, 75, 012 075, <https://doi.org/10.1088/1742-6596/75/1/012075>, 2007.
- Gasparis, G., Lio, A. W. H., and Meng, F.: Surrogate Models for Wind Turbine Electrical Power and Fatigue Loads in Wind Farm, *Energies*, 13, <https://doi.org/10.3390/en13236360>, 2020.

- Guyon, I., Weston, J., Barnhill, S., and Vapnik, V.: Gene selection for cancer classification using support vector machines, *Machine learning*, 46, 389–422, 2002.
- 645 He, R., Yang, H., Sun, S., Lu, L., Sun, H., and Gao, X.: A machine learning-based fatigue loads and power prediction method for wind turbines under yaw control, *Applied Energy*, 326, 120 013, <https://doi.org/https://doi.org/10.1016/j.apenergy.2022.120013>, 2022.
- Hübler, C. and Rolfes, R.: Probabilistic temporal extrapolation of fatigue damage of offshore wind turbine substructures based on strain measurements, *Wind Energy Science*, 7, 1919–1940, <https://doi.org/10.5194/wes-7-1919-2022>, 2022.
- 650 Hübler, C., Weijtjens, W., Rolfes, R., and Devriendt, C.: Reliability analysis of fatigue damage extrapolations of wind turbines using offshore strain measurements, in: *Journal of Physics: Conference Series*, vol. 1037, p. 032035, IOP Publishing, 2018.
- IEC: Wind Energy Generation Systems — Part 1: Design Requirements, Tech. Rep. IEC 61400-1:2019, International Electrotechnical Commission, Geneva, Switzerland, redline version (RLV), including corrigendum 1 (2019-09) and interpretation sheet 1 (2025-02), 2019.
- IEC-61400-1: Wind energy generation systems - Part 1: Design requirements, 2019.
- 655 IEC61400-13: Wind turbines – Part 13: Measurement of mechanical loads, 2021.
- Karadeniz, A.: Advancing harmonic prediction for offshore wind farms using synthetic data and machine learning, *Computers and Electrical Engineering*, 127, 110 613, <https://doi.org/https://doi.org/10.1016/j.compeleceng.2025.110613>, 2025.
- Kinne, M. and Thöns, S.: Fatigue Reliability Based on Predicted Posterior Stress Ranges Determined from Strain Measurements of Wind Turbine Support Structures, *Energies*, 16, <https://doi.org/10.3390/en16052225>, 2023.
- 660 Link, M. and Weiland, M.: Structural health monitoring of the monopile foundation structure of an offshore wind turbine, 2014.
- Miner, M. A.: Cumulative Damage in Fatigue, *Journal of Applied Mechanics*, 12, A159–A164, <https://doi.org/10.1115/1.4009458>, 1945.
- Moynihan, B., Tronci, E. M., Hughes, M. C., Moaveni, B., and Hines, E.: Virtual sensing via Gaussian Process for bending moment response prediction of an offshore wind turbine using SCADA data, *Renewable Energy*, 227, 120 466, <https://doi.org/https://doi.org/10.1016/j.renene.2024.120466>, 2024.
- 665 MVB: Meetnet Vlaamse Banken, accessed: 2025-01-01, <https://meetnetvlaamsebanken.be/>, 2025.
- Noppe, N., Hübler, C., Devriendt, C., and Weijtjens, W.: Validated extrapolation of measured damage within an offshore wind farm using instrumented fleet leaders, *Journal of Physics: Conference Series*, 1618, 022 005, <https://doi.org/10.1088/1742-6596/1618/2/022005>, 2020.
- Pacheco, J., Pimenta, F., Pereira, S., Cunha, A., and Magalhães, F.: Fatigue Assessment of Wind Turbine Towers: Review of Processing Strategies with Illustrative Case Study, *Energies*, 15, 4782, <https://doi.org/10.3390/en15134782>, 2022.
- 670 Pacheco, J., Pimenta, F., Pereira, S., Álvaro Cunha, and Magalhães, F.: Experimental evaluation of strategies for wind turbine farm-wide fatigue damage estimation, *Engineering Structures*, 285, 115 913, <https://doi.org/https://doi.org/10.1016/j.engstruct.2023.115913>, 2023.
- Pedregosa, F., Varoquaux, G., Gramfort, A., Michel, V., Thirion, B., Grisel, O., Blondel, M., Prettenhofer, P., Weiss, R., Dubourg, V., Vanderplas, J., Passos, A., Cournapeau, D., Brucher, M., Perrot, M., and Duchesnay, E.: Scikit-learn: Machine Learning in Python, *Journal of Machine Learning Research*, 12, 2825–2830, 2011.
- 675 Raju, S. K., Periyasamy, M., Alhussan, A. A., Kannan, S., Raghavendran, S., and El-kenawy, E.-S. M.: Machine learning boosts wind turbine efficiency with smart failure detection and strategic placement, *Scientific Reports*, 15, 1485, <https://doi.org/10.1038/s41598-025-85563-5>, 2025.
- Rouholahnejad, F. . and Gottschall, J.: Characterization of local wind profiles: a random forest approach for enhanced wind profile extrapolation, *Wind Energy Science*, 10, 143–159, <https://doi.org/10.5194/wes-10-143-2025>, 2025a.
- 680 Rouholahnejad, F. . and Gottschall, J.: Characterization of local wind profiles: a random forest approach for enhanced wind profile extrapolation, *Wind Energy Science*, 10, 143–159, <https://doi.org/10.5194/wes-10-143-2025>, 2025b.

- Sadeghi, N., D'Antuono, P., Noppe, N., Robbelein, K., Weijtjens, W., and Devriendt, C.: Quantifying the effect of low-frequency fatigue dynamics on offshore wind turbine foundations: a comparative study, *Wind Energy Science*, 8, 1839–1852, <https://doi.org/10.5194/wes-8-1839-2023>, 2023a.
- 685 Sadeghi, N., D'Antuono, P., Robbelein, K., Noppe, N., Weijtjens, W., and Devriendt, C.: Deterministic and probabilistic damage calculation of offshore wind turbines considering the low-frequency fatigue dynamics, in: *Life-Cycle of Structures and Infrastructure Systems*, pp. 3570–3577, CRC Press, 2023b.
- Sadeghi, N., Noppe, N., Morato, P. G., Weijtjens, W., and Devriendt, C.: Uncertainty quantification of wind turbine fatigue lifetime predictions through binning, *Journal of Physics: Conference Series*, 2767, 032 024, <https://doi.org/10.1088/1742-6596/2767/3/032024>, 2024.
- 690 Shafiee, M.: Extending the Lifetime of Offshore Wind Turbines: Challenges and Opportunities, *Energies*, 17, <https://doi.org/10.3390/en17164191>, 2024.
- Simpson, H. A., Chatzi, E. N., and Chatzis, M. N.: A sub-structuring approach to overcome model limitations for input-state estimation of offshore wind turbines, *Journal of Sound and Vibration*, 612, 119 153, <https://doi.org/https://doi.org/10.1016/j.jsv.2025.119153>, 2025.
- Singh, D., Dwight, R., Laugesen, K., Beaudet, L., and Viré, A.: Probabilistic surrogate modeling of offshore windturbine loads with chained Gaussian processes, *Journal of Physics: Conference Series*, 2265, <https://doi.org/10.1088/1742-6596/2265/3/032070>, 2022.
- 695 Sparrevik, P.: Offshore wind turbine foundations state of the art, in: *From Research to Applied Geotechnics*, pp. 216–238, IOS Press, 2019.
- Tewolde, S., Höffer, R., haard, h., and Krieger, J.: Lessons learned from practical structural health monitoring of offshore wind turbine support structures in the North Sea, 2018.
- Velarde, J., Kramhøft, C., Sørensen, J. D., and Zorzi, G.: Fatigue reliability of large monopiles for offshore wind turbines, *International Journal of Fatigue*, 134, 105 487, <https://doi.org/https://doi.org/10.1016/j.ijfatigue.2020.105487>, 2020.
- 700 Weijtjens, W., Noppe, N., Verbelen, T., Iliopoulos, A., and Devriendt, C.: Offshore wind turbine foundation monitoring, extrapolating fatigue measurements from fleet leaders to the entire wind farm, *Journal of Physics: Conference Series*, 753, 092 018, <https://doi.org/10.1088/1742-6596/753/9/092018>, 2016.
- WindEurope: windeurope.org, <https://windeurope.org/wp-content/uploads/files/policy/position-papers/WindEurope-Repowering-and-Lifetime-Extension.pdf>, [Accessed 14-07-2025], 2017.
- 705 Wu, S., Zhang, H., Chen, Z., Liu, X., Zheng, L., Du, M., Li, R., and Li, D.: Experimental Study on Nonlinear Vibrations of Flexible Monopile-Foundation Offshore Wind Turbines in Regular Waves, *Water*, 17, <https://doi.org/10.3390/w17081176>, 2025.
- Zhang, Z., Zhang, W., and Zhang, S.: Strain response prediction of offshore wind turbine tower under free vibration, *Maintenance, Reliability and Condition Monitoring*, 4, 32–43, <https://doi.org/10.21595/marc.2024.23921>, 2024.
- 710 Zhou, Z., Li, X., and Wu, H.: Wind Power Prediction based on Random Forests, <https://doi.org/10.2991/iceeeecs-16.2016.73>, 2016.
- Ziegler, L. and Muskulus, M.: Lifetime extension of offshore wind monopiles: Assessment process and relevance of fatigue crack inspection, 2016.
- Ziegler, L., Smolka, U., Cosack, N., and Muskulus, M.: Brief communication: Structural monitoring for lifetime extension of offshore wind monopiles: can strain measurements at one level tell us everything?, *Wind Energy Science*, 2, 469–476, <https://doi.org/10.5194/wes-2-469-2017>, 2017.
- 715 Ziegler, L., Cosack, N., Kolios, A., and Muskulus, M.: Structural monitoring for lifetime extension of offshore wind monopiles: Verification of strain-based load extrapolation algorithm, *Marine Structures*, 66, 154–163, <https://doi.org/https://doi.org/10.1016/j.marstruc.2019.04.003>, 2019.

Zou, J., Lourens, E.-M., and Cicirello, A.: Virtual sensing of subsoil strain response in monopile-based offshore
720 wind turbines via Gaussian process latent force models, *Mechanical Systems and Signal Processing*, 200, 110488,
<https://doi.org/https://doi.org/10.1016/j.ymssp.2023.110488>, 2023.

Ángel Encalada-Dávila, Vidal, Y., and Tutivén, C.: Strain virtual sensor for offshore wind turbine jacket supports: A time series
transformer approach validated with Alpha Ventus wind farm data, *Mechanical Systems and Signal Processing*, 231, 112653,
<https://doi.org/https://doi.org/10.1016/j.ymssp.2025.112653>, 2025.